Two Modifications Formed by "Sulflower" $C_{16}S_8$ Molecules, Their Study by XRD and Optical Spectroscopy (Raman, IR, UV−Vis) Methods

Sergey S. Bukalov,[†] Larissa A. Leites,[†] Konstantin A. Lyssenko,*[,†] Rinat R. Aysin,[†] Alexander A. Korlyukov,[†] Jan V. Zubavichus,[†] Konstantin Yu. Chernichenko,[‡] Elizabeth S. Balenkova,[‡] Valentine G. Nenajdenko,[‡] and Mikhail Yu. Antipin[§]

A. N. Nesmeyanov Institute of Organoelement Compounds, Russian Academy of Sciences, 28 Vavilova street, 119991 Moscow, Russia, Department of Chemistry, Moscow State University, Leninskiye Gory, 119992 Moscow, Russia, and Department of Natural Sciences, New Mexico Highlands University, Las Vegas, New Mexico 87701

Received: July 11, 2008; Revised Manuscript Received: August 4, 2008

Sublimation of sulflower, octathio[8]circulene $C_{16}S_8$ (**1**), on heating under high vacuum ($\sim 10^{-5}$ Torr) leads to successive formation of two modifications: a white film (**1W**) and a red polycrystalline solid (**1R**). When kept at room temperature for several weeks, **1W** spontaneously turns pink, reflecting the monotropic phase transition **1W** → **1R**. The accurate molecular and crystal structure of **1R** has been studied using low-temperature (100 K) high-resolution single crystal X-ray analysis. The $C_{16}S_8$ molecule in crystal is strictly planar with nearly equalized bonds of each type (C−C, C−S, and C═C). The point symmetry group of the free molecule is D_{8h}, and the crystal space group is $P2_1/n$. These data allowed group-theoretical analysis of vibrational normal modes to be accomplished. Investigation of the charge density distribution of **1R** including Bader's AIM approach has revealed rather strong intermolecular S···S, S···C, and C···C interactions of charge transfer and π-stacking types with overall lattice energy of 28.5 kcal/mol. The charge transfer due to the S···S interactions is the reason for the red coloration of **1R**. The latter is reflected by its UV−vis spectrum exhibiting absorption bands in the visible region which are absent from that of **1W**. Both modifications were studied comparatively by vibrational (Raman, IR) and electronic spectroscopies as well as XRD powder diffraction. All the results obtained are fully consistent and show that **1W** is much less ordered than **1R** with significantly weakened intermolecular interactions. Rationalizing of these results has led to an idea that **1W** could be soluble, in contrast to **1R**. Indeed, **1W** appeared soluble in common solvents; this finding opens the way to the study of the chemistry of **1** and investigation of its electrooptical properties.

Introduction

There is currently great interest in creating new materials with valuable electronic and optical properties. Organosulfur compounds such as tetrathiafulvalenes and annulated π-conjugated β-oligothiophenes hold much promise in this respect due to their potential applications as organic thin-film transistors,[1] OLEDs,[2] and other[3] devices.

The properties of β-oligothiophenes containing three and four,[4,5] as well as three, seven, and eleven[6−9] fused thiophene rings, are the most studied. In a series of comprehensive publications of the Rajca group,[6−9] it was emphasized that in these oligomeric structures the annulated thiophene rings are located in such a manner that all sulfur atoms are positioned at the molecular periphery, thus favoring formation of two- (2D) and three-dimensional (3D) associates by means of shortened intermolecular S···S contacts. Such a type of supramolecular moieties possesses enhanced transport properties, important for the design of industrially valuable materials (see ref 9 and references therein).

It is evident that, from the point of view of 3D-structure formation, the most promising would be circulene-type molecules. Indeed, in 2006 three of us reported the synthesis and some properties of the first representative of a new class of compounds—fully heterocyclic circulenes, octathio[8]circulene $C_{16}S_8$ (**1**)—whose highly symmetrical planar structure was suggested on theoretical grounds and on the basis of X-ray powder diffraction and solid-state MAS ^{13}C NMR data.[10] As molecule **1** resembles a blooming sunflower, it was proposed to call it "sulflower" (from "sulfur" and "flower"). The discovery of this beautiful molecule of a novel type has aroused much interest. In particular, sulflower was speculated to be effective as a hydrogen storage material.[11] Due to the planar π-conjugated structure of molecules **1** and their extremely close packing in the solid state with strong intermolecular interactions,[10] the substance **1** might show prospect as a potential material in microelectronics, nanotechnology, and materials science investigations. Indeed, a recent quantum-chemical calculation[12] of sulflower reorganization energy—an important parameter for organic semiconducting systems—has indicated increasing sulflower capability as a potential organic semiconductor.

However, the full and unequivocal structural and spectroscopic characteristics of **1** are still lacking and its proposed applications are limited due to its previously reported[10] insolubility in organic solvents. That is why it seems necessary to further elucidate the molecular and crystal structure of **1** as well as optical spectra in relation to its physicochemical properties.

* Corresponding author. E-mail: kostya@xray.imeos.ac.ru.
[†] A. N. Nesmeyanov Institute of Organelement Compounds, Russian Academy of Sciences.
[‡] Moscow State University.
[§] New Mexico Highlands University.

10.1021/jp806134u CCC: $40.75
Published on Web 10/07/2008

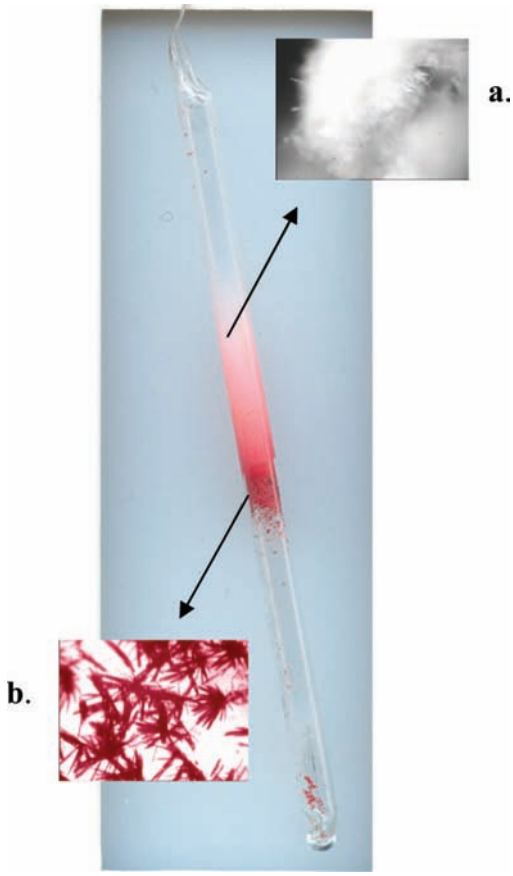

Figure 1. One of numerous results of sublimation of $C_{16}S_8$ substance in a capillary (d = 5 mm). Microphotographs of the (a) white (**1W**) and (b) red (**1R**) parts (magnification 50×).

Results and Discussion

Peculiarities of the Sample Sublimation. The substance **1** was previously isolated as a dark-red powder insoluble in common organic solvents.[10] In the course of our study, a sample of **1,** prepared as described in ref 10, was repeatedly sublimed in glass capillaries under high vacuum ~10^{-5} Torr. Interestingly, the results obtained appeared to be rather unexpected. Under the conditions used, the substance starts to sublime on heating to 200 °C and deposits on the upper part of the capillary as a white film (Figure 1). On further heating, the sublimed substance is located beneath and gradually acquires a bright cherry-red color. Closer examination of the white and red parts under the microscope (Figures 1 and 2) shows that the white film seems to be amorphous, cottonlike by sight, whereas the red part is evidently microcrystalline, consisting of tiny needles and their "bundles". Thus, the substance **1** obviously exists in two different modifications. Hereafter we will denote them as **1W** and **1R.** The largest single crystals of **1R** were exposed to X-ray crystallography. Both modifications **1W** and **1R** were studied by powder X-ray diffraction as well as by Raman, IR, and UV−vis spectroscopies. All the results are mutually consistent and evidence that **1W** is less ordered (see below). When kept at room temperature for several weeks, the white film spontaneously and gradually turns pink, thus indicating that modification **1W** could be metastable. If so, the phase transition **1W** → **1R** of ordering type is monotropic.

X-ray Diffraction Study of Molecular and Crystal Structure of 1R. According to X-ray diffraction analysis, a molecule of **1** in crystal **1R** occupies the special position—center of inversion (Figure 3, Table S1 in Supporting Information)—and is planar with root-mean-square deviation of atoms from the molecular plane being as small as 0.006 Å. The inner eight-membered cycle is characterized by almost equal bond lengths varying in the range 1.420(1)−1.417(1) Å. The same equalization of lengths is observed for two other types of bonds: S−C [1.7450(7)−1.7554(8) Å] and C═C [1.379(1)−1.381(1) Å] in the fused thiophene rings. Comparison of geometric parameters of **1** with the corresponding ones in its formal "half"—thieno[2,3-*b*]thieno[3′,2′:4,5]thieno[3,2-*d*]thiophene[4]—clearly shows that in the latter the S−C bonds of the "center" thiophene rings are slightly shorter [1.733−1.736(2) Å], the C═C bonds are almost the same [1.380(3) Å], and the C−C ones are elongated up to 1.434(3) Å. Thus we can conclude that formation of the inner eight-membered ring in **1** only slightly affects the S−C and C−C bond lengths and does not practically change the C═C ones.

Analysis of crystal packing has revealed that molecules in **1R** are assembled into a three-dimensional framework by means of three types of shortened contacts: C···C between the carbon atoms of π-systems, S···C between the S atoms and the C atoms of π-systems inside the columns (directed along crystallographic axis a), and C−S···S−C contacts holding these associates together (Figure 4). It is notable that the geometric parameters alone seem sufficient to propose that the π-stacking interactions are significantly weaker than the S···S ones. Indeed, the interplane distance between the molecular planes in the columns is 3.497(1) Å, while the S···S contacts are significantly shorter [3.187(1)−3.540(2) Å]. It should be noted that the latter are even shorter that the S···S contacts (3.330−3.564 Å) observed for a related compound: [7]helicene (β-heptathiophene).[9] Furthermore, shortened C−S···S−C contacts are characterized by specific directionality, i.e., the majority of the corresponding SSC angle values are close to the value of 180°, expected for such a type of interaction (see, e.g., ref 13). At the same time, a considerable degree of π-system overlap (Figure 4) can partly compensate an increase in the S···C interatomic distances as compared to the S···S ones.

Taking into account that the number and strength of the S···S, S···C, and C···C interactions for independent atoms in **1R** are different, in particular, the S(3) atom is involved in only one S···S interaction, we can assume that small variations in the values of intramolecular bond lengths and angles in **1R** can be a consequence of crystal packing effects.

Vibrational Spectrum. ***Group-Theoretical Analysis of Normal Modes.*** The isolated planar molecule **1** belongs to the D_{8h} point symmetry group of the order 32. To our best knowledge, the only species of the same symmetry is cyclooctatetraene ring in its complexes with metal ions.[14] The results of group-theoretical analysis[15] show that the 66 normal modes of molecule **1** are distributed among the symmetry species as follows:

$$\Gamma_{vib} = 3A_{1g}(R) + 2A_{2g} + 3B_{1g} + 3B_{2g} + 2E_{1g}(R) + 6E_{2g}(R) + 3E_{3g} + 0A_{1u} + 2A_{2u}(IR) + 2B_{1u} + 1B_{2u} + 5E_{1u}(IR) + 3E_{2u} + 6E_{3u}$$

The vibrational spectrum of the centrosymmetric molecule **1** should obey the mutual exclusion rule; this means that no normal modes may be active in both IR and Raman spectra. According to the selection rules for D_{8h} symmetry, Raman-active modes are totally symmetric modes of A_{1g} species and also doubly degenerate modes of E_{1g} and E_{2g} species. Thus, the Raman spectrum of the free molecule **1** may exhibit, in principle, 11 lines. Accordingly, only A_{2u} and E_{1u} species are IR active; that is, seven bands may appear in the IR spectrum. All the other

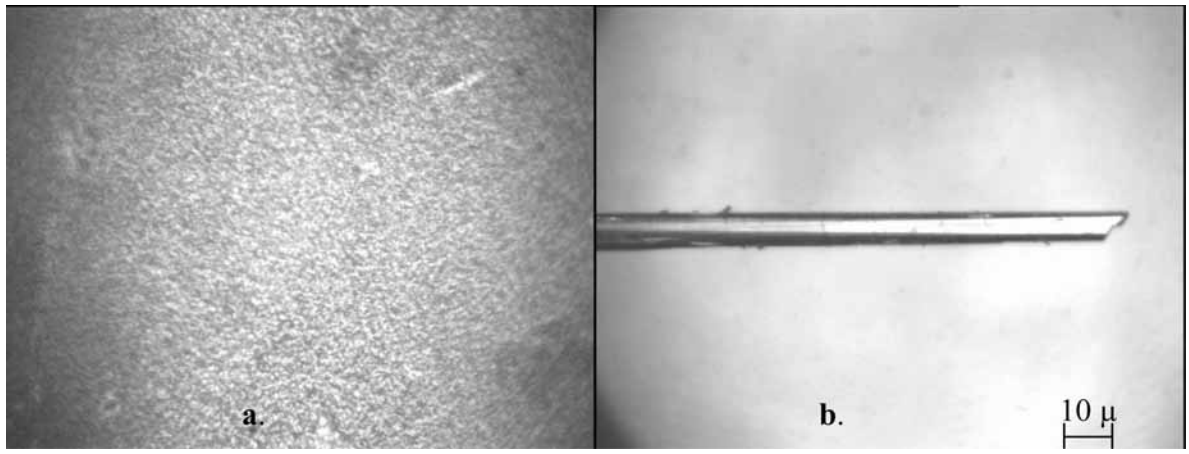

Figure 2. Comparison of microphotographs of a white film **1W** (a) and a red microcrystal **1R** (b).

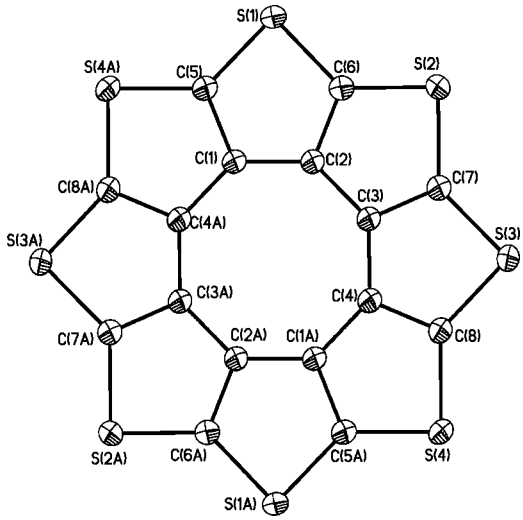

Figure 3. General view of molecule **1** in presentation of atoms by thermal ellipsoids ($p = 90\%$). Atoms with label "A" are obtained from the basic ones by inversion center.

normal modes are forbidden. It is important to note that normal modes belonging to different symmetry species but possessing close eigenvectors could exhibit close frequency values.

The X-ray data obtained for the single crystal of **1R** indicate that $Z = 2$ and the space group is $P2_1/n$. The factor group of the latter is isomorphous to the C_{2h} point group. From these results, it follows unambiguously that the site symmetry of the molecule in the lattice is C_i. Correlation among the symmetry groups D_{8h}, C_i, and C_{2h} is depicted in Figure 5.

Based upon these data, all *gerade* modes of the isolated molecule should grade into A_g species and all *ungerade* modes into A_u species of the site group with degeneracy lifting. Then, due to resonance interaction of two molecules in the unit cell, each of the A_g and A_u modes of the site group should transform into a Davydov doublet (correlation field splitting). Each A_g mode should give rise to Raman-active components A_g and B_g, while each A_u mode should give rise to IR-active components A_u and B_u of the factor group C_{2h}, correspondingly. Thus, the mutual exclusion rule should hold true also in the spectrum of the crystal **1R**. However, if the intermolecular interactions in the molecular crystal were weak, the effects of molecular symmetry lowering in the crystal could be small and it would be possible to describe the spectrum of the crystal using an oriented gas model.

Normal Coordinate Analysis (NCA). Quantum-chemical calculations of normal-mode frequencies and eigenvectors (in a harmonic approximation) and also of Raman and IR intensities for the free molecule were carried out at the DFT/PBE level of theory. The resulting simulated spectra are presented in Figures 6 and 7. Agreement between the calculated and experimental frequencies is satisfactory without any scaling; there are some precise coincidences and some differences within the limits of $15-20$ cm^{-1}.

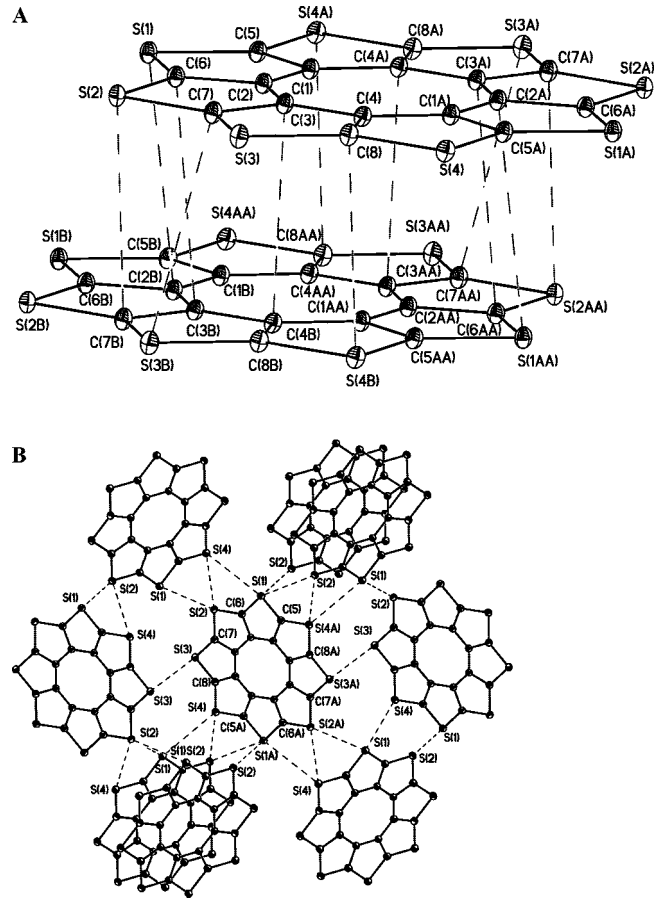

Figure 4. Fragments of crystal packing of **1R** illustrating the stacking interactions (A) and the S···S contacts (B). For simplicity, in (B) the atoms obtained from the basic ones by various symmetry operations are shown without additional labels.

Experimental Raman and IR Spectra and Their Discussion. We were not able to obtain the IR spectrum from the pure sample of **1W** because the sublimed white film turns pink in the spectrometer under the influence of IR irradiation. The IR spectrum obtained for the pink film appeared much the same

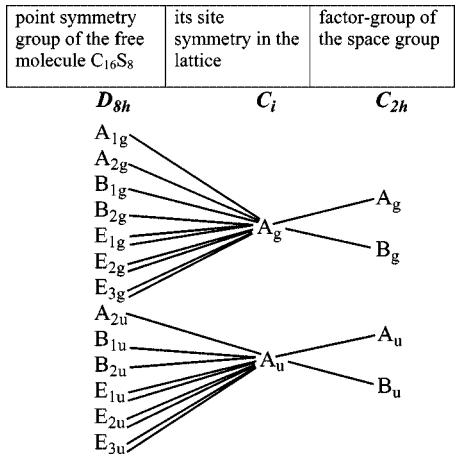

Figure 5. Correlation among the irreducible representations of the point symmetry group of the free molecule $C_{16}S_8$ (D_{8h}), its site symmetry in the crystal lattice (C_i), and the factor group (C_{2h}) isomorphous to the crystal space group $P2_1/n$.

as that obtained for the sample of **1R**. The spectrum presented in Figure 6 somewhat differs from that reported in ref 10; the absence of an intense band at 725 cm^{-1} and also of weak bands at 1709, 2854, and 2924 cm^{-1} is especially notable. Analysis of numerous Raman spectra obtained has shown that the spectra of **1R** somewhat differ from those of **1W**. Let us denote them R-**1R** and R-**1W**. The R-**1R** spectrum contains more lines than the R-**1W** one (Figure 7).

The experimental and computed results obtained are juxtaposed in Table S2 of the Supporting Information, where an assignment of normal modes to symmetry species and to particular vibrational motions is presented.

Ungerade Modes. The data obtained allow confident assignment of all the ungerade modes of the free molecule, both IR active and forbidden. According to NCA calculations, the two IR-active modes of A_{2u} species should have the following frequency (cm^{-1}) and intensity (in parentheses; km/mol) values: 97 (2) and 502 (27). These modes are symmetric atomic deviations from the plane formed by eight central C−C bonds. (See Figure 8, where the shapes of the molecular motions belonging to the given normal modes in the extreme phase of vibration are depicted with strongly exaggerated vibrational amplitudes for better illustration. Analogous patterns for A_{1g} modes are given in Figure 9; the remaining normal modes can be found in the Supporting Information.)

We could not register the IR band corresponding to the first A_{2u} mode for technical reasons. The second one was observed as a very intense IR band at 500 cm^{-1} (Figure 6). Analogously, experimental frequency and intensity values of the five IR bands attributable to IR-active doubly degenerate E_{1u} species are in good accord with their calculated values (Table S2 in the Supporting Information). All these modes are in-plane vibrations involving various distortions of the molecule (see the Supporting Information). Note the splitting into Davydov doublets of the intense IR bands at ∼950 and 657 cm^{-1}. The calculated frequencies of the IR-inactive ungerade modes are given in Table S2 in the Supporting Information. It is important to note that they have no experimental IR counterparts. Thus, the main features of the IR spectrum agree well with the selection rules of the D_{8h} symmetry. Degeneracy does not lift; inactive modes are not observed. However, there are some "extra" very weak IR bands (see Figure 6), whose origin is unclear. It is of importance that they do not correspond either to forbidden ungerade modes (except for 726 cm^{-1}), or to any gerade fundamentals. They could be ascribed to various overtones and combinations with the participation of forbidden modes as well as to vibrations outside the Brillouin zone center ($k \neq 0$) owing to the finite, very small crystal size. As a whole, the IR spectrum appears not very sensitive to the crystal field effects: the only manifestation of the latter is correlation field splitting of the two bands.

Gerade Modes. According to the NCA calculation for the free molecule, three totally symmetric vibrations have the following frequencies (cm^{-1}) and intensities (in parentheses; arbitrary units): 337 (52), 819 (25), and 1404 (720). In the Raman spectra of both types they are easily identified as the lines at 345s, 829ms, and 1403vs. In accordance with the theory, their intensity concurrently decreases when the polarization plane of the exciting beam is turned over 90°. The forms of these normal modes are given in Figure 9.

In particular, the mode at 337 cm^{-1} is the in-plane expansion of the whole molecule, that is, a simultaneous stretching of all the C−S and C−C bonds with small participation of the C═C bonds and angle deformations; it is a "breathing" or "pulsation" mode. According to the computed potential energy distribution (PED), contributions from the ν_{C-S} and ν_{C-C} coordinates into the potential energy of this normal mode are 48% and 32%, respectively. The frequency 819 cm^{-1} belongs to a complex mode, during which the C−S and C−C bonds are stretching in an opposite manner: the C−S bonds lengthen as the C−C bonds contract, this being accompanied by a corresponding decrease in the CSC angles. The contributions from the ν_{C-S} and ν_{C-C} coordinates into the PED of this mode are 32% and 24%, respectively; the remaining contributions are due to angle deformations, whereas the C═C bonds do not participate at all. The normal mode at 1404 cm^{-1} is predominantly the $\nu_{C=C}$ stretch (72% in PED); that is why it manifests itself as the most intense Raman line, with the polarizability change during this vibration being the greatest. The eigenvector of this mode involves C═C bond stretching with simultaneous decrease in the CSC angles and a slight lengthening of the C−C bonds. Thus the A_{1g} modes are of mixed stretching−deformational origin; none of them is localized in a single set of equivalent coordinates.

Six in-plane degenerate Raman-active modes of E_{2g} species were calculated as 250 (10), 329 (9), 616 (20), 983 (4), 1295 (37), and 1475 (261), and easily assigned as lines at 255w, 339s, 630w, 1004w, 1295vw, and 1479s. Two out-of-plane degenerate modes of E_{1g} species may also be Raman active. However, their eigenvectors are close to those of E_{3g} modes, also degenerate and out-of-plane, but silent. The choice between them is not unambiguous. NCA calculation results in 232 (3) and 514 (0.5) for E_{1g} modes and 153, 247, and 707 for silent E_{3g} modes. In the R-**1R** spectrum, four lines are observed below 600 cm^{-1}: 148 w, 222m, 275w, and 518mw. Thus it is evident that two E_{3g} modes, inactive for the isolated molecule, appear in the spectrum of the crystal.

Detailed analysis of symmetry-forbidden gerade modes can be found in the Supporting Information. It is important that some of them (those of A_{2g}, B_{1g}, and B_{2g} species) manifest themselves as weak and very weak Raman features in the spectrum of **1R**. Thus, the salient Raman lines agree well with theoretical predictions for the free molecule of D_{8h} symmetry. However, in the R-**1R** spectrum some weak lines, corresponding to forbidden gerade modes, are also observed, reflecting molecular symmetry lowering in the crystal lattice. For some Raman lines of **1R**, in contrast to those of **1W**, splitting in doublets is also notable (Figure 10), analogous to that observed in the IR

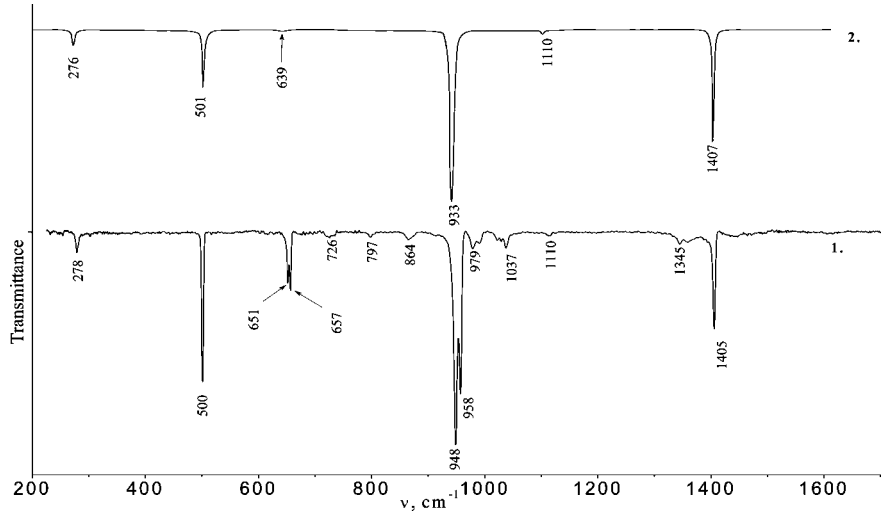

Figure 6. Experimental IR spectrum (with baseline correction) of a red sample of $C_{16}S_8$ (1) in comparison with that calculated for the free molecule (2).

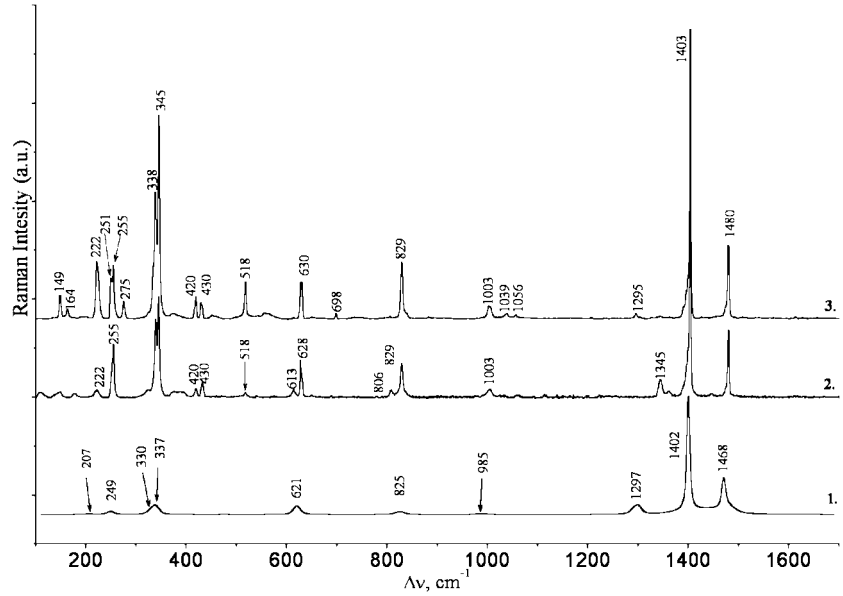

Figure 7. Comparison of the simulated Raman spectrum (1) of the free sulflower molecule with the experimental ones obtained for the white (2) and red (3) modifications; excitation line 632.8 nm.

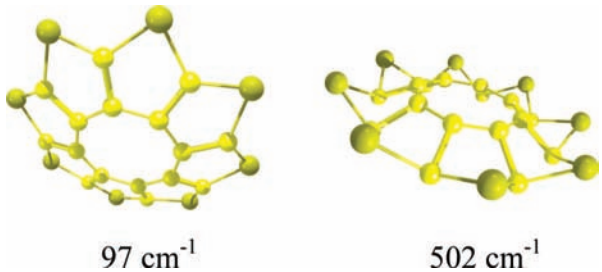

Figure 8. Calculated frequencies (cm^{-1}) and forms of molecular motions of the IR-active out-of-plane *ungerade* A_{2u} modes.

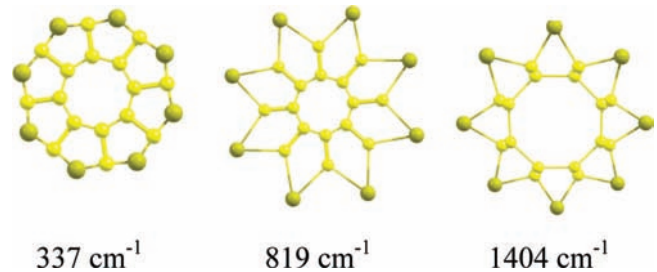

Figure 9. Calculated frequencies (cm^{-1}) and forms of the Raman-active totally symmetric in-plane modes of A_{1g} species.

spectrum. Examining of these mode eigenvectors reveals that they involve large displacements of S atoms. The Davydov splittings observed could be due to significant intermolecular S···S interactions, found in **1R** by the X-ray method. In the R-**1W** spectrum, the lines at 148, 222, 275, and 518 cm^{-1} disappear or become very weak (Figure 7). It is clear that the R-**1W** spectrum is closer to that of the free molecule and belongs to a less ordered modification with weakened intermolecular interactions.

However, for some sublimed samples we observed Raman spectra, intermediate between R-**1R** and R-**1W**; these samples evidently contain both modifications. In all the Raman spectra obtained, some very weak "extra" bands were observed, e.g., 1345 cm^{-1}, whose origin is as vague as for those in the IR spectrum. It is interesting that the Raman spectrum appears more "sensitive" to the crystal field effects than the IR spectrum. On the whole, it is very important that the vibrational spectrum does not show degeneracy lifting and does not violate the mutual

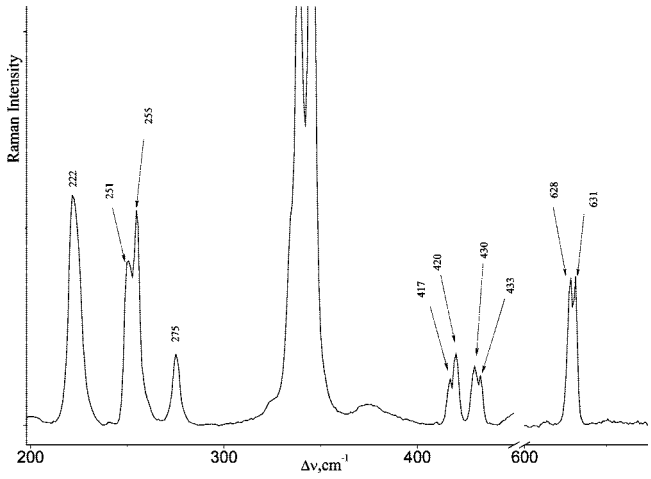

Figure 10. Detailed illustration of the Davydov splittings of some lines in the Raman spectrum of **1R**.

exclusion rule. This agrees well with highly symmetrical planar structure of molecule **1**, established by the X-ray analysis.

It is pertinent to mention here that the vibrational frequencies of thiophene ($\nu^{s}_{C=C}$ 1406, $\nu^{as}_{C=C}$ 1532, ν^{s}_{C-S} 833, ν^{as}_{C-S} 868 cm^{-1}) are very close to those of sulflower. Vibrational spectra of some annulated β-olgothiophenes have been reported,[5] but it is difficult to compare them with those of sulflower due to different symmetry and selection rules for these molecules.

Electronic Absorption Spectrum. Quantum-chemistry calculation of electronic energy levels of the free molecule resulted in the following values of the lowest-energy electronic transitions: 43 480 cm^{-1} (230 nm), 36 364 cm^{-1} (275 nm), and 30 864 cm^{-1} (324 nm). This means that molecule **1** should not absorb light in the visible region. Notably, the UV−vis spectra of related compounds, β-oligothiophenes published by Rajca et al.,[7−9] even of the largest one—helically annulated β-undecathiophene—also exhibit no absorption above 350 nm.

We succeeded in obtaining experimental UV−vis spectra of the solid sulflower. The samples of **1W** were white films freshly sublimed on quartz plates under the conditions described above, and those of **1R** were prepared just by smearing and pressing the red polycrystalline substance between two quartz plates. In the spectrum of solid **1W**, the absorption contour subjected to curve-fitting analysis exhibits λ_{max} at 206, 244, 277, and 308 nm (Figure 11.2a). In contrast, the spectra of all the red samples evidently contain weak but distinct absorption in the visible region, at ∼420 and ∼530 nm (Figure 11.3).

This is an obvious reason for the red color. Thus, a conclusion can be drawn that the coloration of **1R** is caused only by strong intermolecular interactions in the crystal, and it is not immanent to the free molecule **1**. The UV−vis spectra of solid pink samples are intermediate between those of white and red ones, showing that the former are mixtures of **1W** and **1R**. This is seen from the curve b in Figure 11.2, where an evident blue shift of the absorption contour is observed due to an admixture of **1R**.

X-ray Powder Diffraction Study of the Two Modifications. To rationalize the experimentally observed spectroscopic differences between the red polycrystalline powder **1R** and the sublimed thin white films **1W**, both types of samples have been characterized by X-ray powder diffraction at room temperature. The experimental patterns of two representative samples (Figure 12) are compared with previously published data[10] and with a simulated pattern calculated in terms of the low-temperature single crystal data. Significant changes in the reflection intensities are obvious.

According to the calculation, the highest intensity is expected for the reflection (120) at a scattering angle of ca. 25.5°. Meanwhile, this peak is nearly absent in the case of **1R** and is noticeably suppressed in the case of **1W**. On the other hand, the intensities of first two reflections, viz., 011 and 002, are notably increased for both samples compared to the theoretical pattern. In general, peaks with zero h and nonzero l Miller indices prevail in both patterns and the trend is more pronounced for **1R**. These differences between the calculated and experimental patterns strongly indicate a preferred orientation of crystallites in both samples with the crystallographic axis c nearly parallel to the substrate surface and the axis a preferably perpendicular to it. A preferred orientation is typical of powders composed of crystallites with strongly anisotropic shapes. The crystals **1R** are predominantly needle-shaped (Figure 2b). Most probably, the habitus long axis corresponds to the crystallographic axis c. Interestingly the film **1W** demonstrates the same type of preferred orientation but pronounced to a lesser extent, probably due to smaller crystallite sizes (see below). There is some difference between the positions of peaks in the patterns of **1W** and **1R**. Moreover, the diffraction pattern of **1W** is characterized by significantly broader reflections with intensities rapidly decreasing with an increase in the scattering angle. Parameters of the diffraction peaks of the two modifications are summarized in Tables S3 and S4 in the Supporting Information. In particular, the reflection (031) is shifted by as much as ca. 0.25° to smaller angles and is 3 times broader in **1W** compared to **1R**. This effect is probably related to some specific structural disorder realized in the film. Analysis of the crystal packing in **1R** indicates that the (031) crystallographic plane passes through the molecular inversion center. Consequently, the broadening and shift of this peak for **1W** can be associated with restricted rotation (libration) of the molecules in the corresponding plane due to weakening of the structure-forming intermolecular S···S contacts. The average coherent scattering lengths for different crystallographic directions in **1R** and **1W**, estimated for all the reflection observed at $2\Theta < 32°$, are ∼700 and ∼200 Å, respectively. Refinement of the unit cell parameters versus experimental diffraction data for **1R**, taking the single crystal data as a starting approximation, yields the values $a = 3.915(3)$, $b = 16.586(4)$, $c = 11.171(4)$ Å, $\beta = 94.4(2)°$, and $V = 723.3$ Å^3 for 36 reflections with no systematic absence violation from the $P2_1/n$ space group [$F(20) = 26$, $F(20)' = 33$, maximum 2Θ deviation lower than 0.05°]. These parameters are reasonably close to those obtained from the single crystal diffraction data, taking into account the thermal expansion on going from 100 K to room temperature. Thus, it is evident from the powder X-ray diffraction (XRD) data that the white modification is less ordered than the polycrystalline red powder, with the S···S intermolecular interactions in the former being weakened.

Investigation of Charge Density Distribution and Estimation of Interaction Energy in 1R on the Basis of High-Resolution XRD Data. Although the geometric data alone can hardly serve as a measure of interaction energy and even as an unambiguous indicator of bonding, the precise XRD data can provide definite answers to these questions. Recently we have demonstrated that high-resolution single crystal XRD analysis gives an extraordinary opportunity to estimate directly the contribution of intermolecular interactions to the crystal lattice energy ($E_{lattice}$) on the basis of experimental data.[14] Estimation of the intermolecular contact energy is based on topological analysis of the electron density distribution function $\rho(\mathbf{r})$ in crystals within Bader's "atoms in molecules" (AIM) theory,

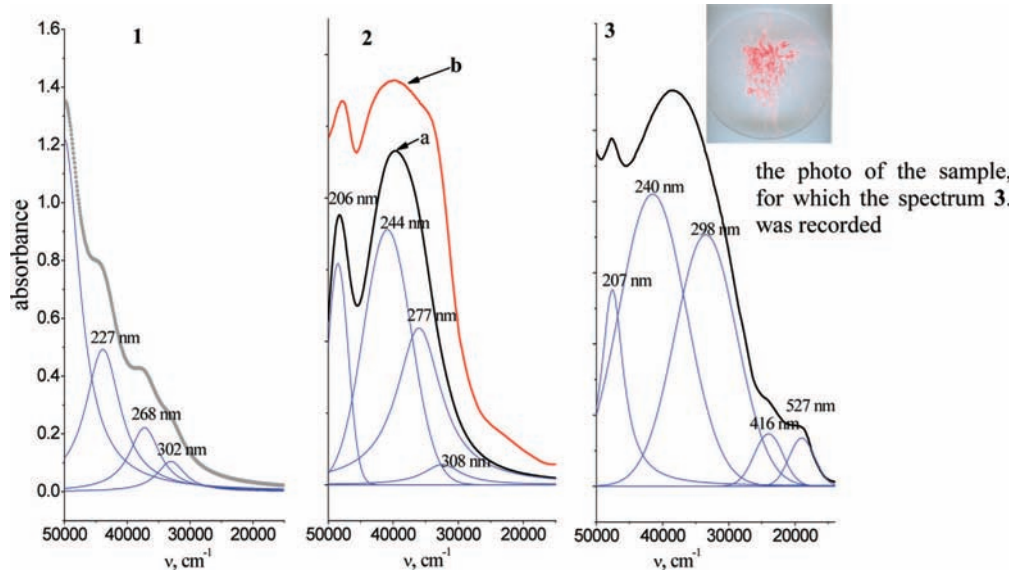

Figure 11. UV−vis spectra of sulflower and their computer curve-fitting analyses: (1) solution of **1W** in hexane; (2) (a) freshly sublimed white film **1W** (sublimation time 2.5 min) and (b) the same sample after 1 month; (3) red crystals of **1R** smeared and pressed between quartz plates.

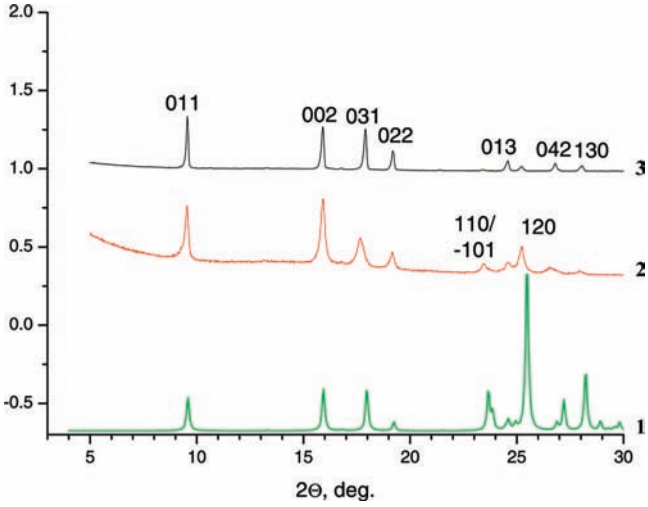

Figure 12. Powder X-ray diffraction patterns of sulflower: (1) theoretical pattern calculated from X-ray single crystal data for **1R**; (2) experimental pattern obtained for white film **1W** sublimed on a silicon plate; (3) experimental pattern obtained for **1R** powder placed on a silicon plate.

which makes it possible to clearly distinguish between bonding interactions and intermolecular contacts.[15] The AIM theory has been applied both experimentally and theoretically to a wide variety of structures containing many different types of intermolecular interactions,[16] including the π-stacking and S···S ones.[17−19] The energy of bonding interactions is estimated using the correlation found between the energy of the contact (E_{cont}) and the value of the potential energy density function $v(\mathbf{r})$ in the corresponding bond critical point (3,−1).[20] As a validation of accuracy of this approach, a good agreement can serve between the $E_{lattice}$ values obtained by us and the experimental values of the sublimation enthalpy $\Delta H°_{subl}$.[14]

The correctness of the charge density distribution function for **1** obtained within the multipole refinement can be illustrated to some extent by analysis of deformation electron density (DED) maps. Indeed, the DED map of the molecular plane of **1** is characterized by the expected features: the uniform distribution of the DED with almost the same maxima of positive DED values for the C−C bonds of the inner ring and for the fused thiophene cycles (Figure 13A). The charge accumulation for the C−C and S−C bonds does not contain any undesirable "double peaks" (as, e.g., those in ref 17 which are in fact a consequence of incorrect kappa values). It should be noted that electron lone pairs (Lp's) of sulfur atoms are located above and below the molecular plane as, e.g., can be seen in the section of DED perpendicular to the five-membered-ring plane and passing through the S(1) atom and the center of the C(1)−C(2) bond (Figure 13B). These maxima in the isolated molecule must a priori be equal, but in the crystal, one of them is approximately 2 times higher than the other. Such a difference in maximum DED heights that formally correspond to Lp's can be a consequence of intermolecular contacts in the crystal with participation of S(1) atoms (see Figure 4B). In addition, the latter section clearly shows that the C−C bond of the inner ring is characterized by a pronounced π-component that is reflected by its elliptical shape (Figure 13B).

A critical point (CP) search for **1** has revealed the presence of both expected CPs (3,−1) for all the C−C, C═C, and C−S bonds and CPs (3,+1) for the five- and eight-membered rings; thus the characteristic set of CPs for **1** meets the Poincaré−Hopf relationship.[15] The topological parameters for chemical bonds of each type in the symmetrically independent part of the molecule vary within the narrow limits (see Table S5 in the Supporting Information). The results obtained for the five-membered rings (taking into account the differences in bond lengths) are close to the corresponding values for the thiophene ring in the angiotensin II receptor antagonist.[21] It should be noted that although the eight-membered ring is formally antiaromatic, the values of its ellipticity (ε) that can serve in the given case as a measure of π-component contribution are rather high (0.17−0.29) and in average are only slightly less than those for the C═C bonds in the five-membered ring (0.20−0.32). For comparison, the ε values for the S−C bonds are 0.13−0.30. A wide range of ε values can also be a consequence of crystal packing effects. Some information concerning the degree of delocalization of π-density in molecule **1** can be also obtained from the analysis of eigenvalues in CPs (3,+1).[22] The latter measure of aromaticity is based on the analysis of the absolute value of a unique negative eigenvalue ($|\lambda_1|$) of the Hessian matrix corresponding to the curvature of the $\rho(\mathbf{r})$ perpendicular to the

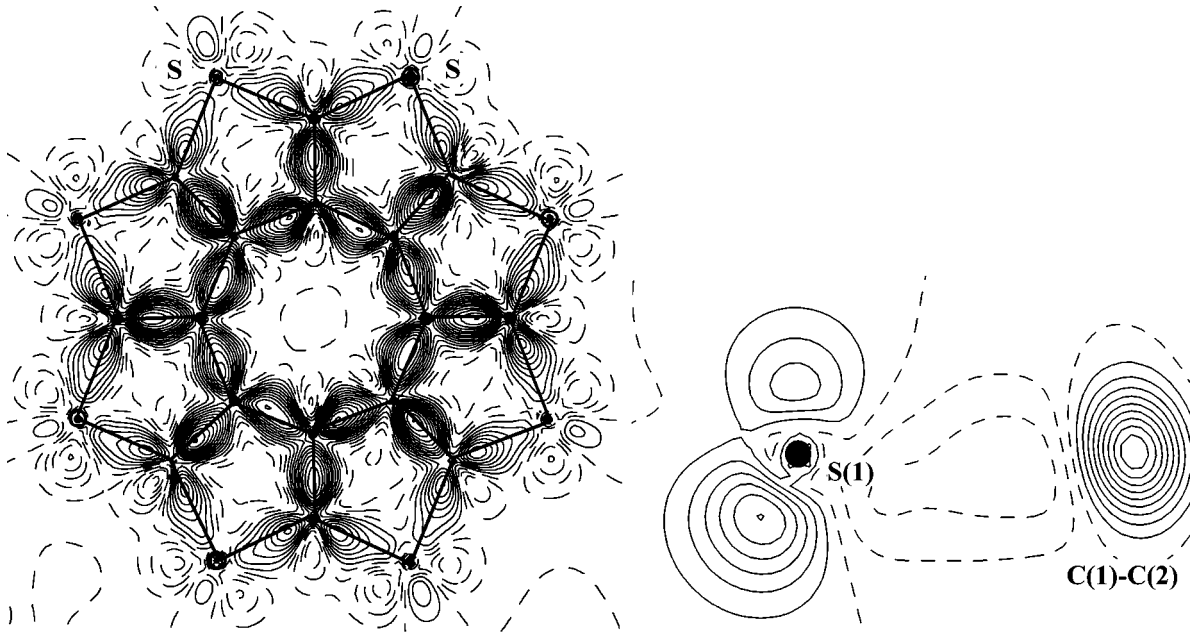

Figure 13. Deformation electron density (DED) maps in the molecular plane (A) and in the section passing through the S(1) atom and the center of the C(1)−C(2) bond (B). Contours are drawn with a 0.05 e Å^{-3} step. Negative values for DED maps hereinafter are shown by dashed lines.

molecular plane. According to the criteria mentioned, an increase in aromaticity can be clearly seen from the comparison of the ($|\lambda_1|$) values in the CPs (3,+1) for rings of different sizes. Taking into account that the value of $|\lambda_1|$ depends on the ring size (see Table S5 in the Supporting Information), we have used the relative value $|\lambda_3/\lambda_1|$. For thiophene cycles of **1,** this ratio is significantly higher (13.8) than that for the eight-membered inner ring (10.6), thus indicating a higher degree of π-delocalization in the former.

With this in mind, it was of interest to calculate for the cross-conjugated sulflower molecule its NICS (nuclear independent chemical shift) index that was first proposed as a measure of aromaticity by von R. Schleyer et al. in 1996,[23] refined in refs 24 and 25, and is widely used now. The isotropic indices NICS(1) (i.e., at points 1 Å above the ring centers to exclude in-plane contributions), rather than more sophisticated NICS(1)$_{zz}$, were chosen for simplicity. The NICS(1) value above the eight-membered central ring is +2.4; this means that the ring is antiaromatic. Above each of the thiophene cycles, NICS(1) = −7.35; this negative value denotes ring aromaticity. Thus, the NICS values confirm the expected "aromatic−antiaromatic" nature of the molecule studied and are in good accord with the electron density data presented above. Notably, for thiophene itself the NICS(1) is equal to −10.2.[24] The NICS indices of **1** reported recently[12] are qualitatively similar, but the exact values differ from ours because they were calculated with the dummy atom at the ring centers.

It should be noted that such integral parameters of atoms as their volumes and charges are also slightly different for equivalent atoms, thus being affected by crystal packing. The volumes, electronic population, and Lagrangian of the $\rho(\mathbf{r})$ were integrated over the atomic basins (Ω) surrounded by the zero-flux surface (Table S6 in the Supporting Information). Although the integrated value of the Lagrangian [$L(\mathbf{r}) = -1/4\nabla^2\rho(\mathbf{r})$] for every $\mathbf{\Omega}$ has to be exactly 0,[25,26] reasonably small numbers with an averaged value of 1.2×10^{-5} au were obtained. The maximum $L(\mathbf{r})$ value was obtained for the C(6) atom (1.4×10^{-4} au). The atomic charges estimated according to this procedure lead to charge leakage equal to 0.001 e. The sum of atomic volumes in the crystal (177.15 Å^3) reproduces the independent part (0.25) of the unit cell volume [117.23(2) Å^3] with a small error of 0.06%. As one can see from Table S6 in the Supporting Information, the atoms C(5)−C(8) attached to the sulfur atoms are all characterized by a negative charge (−0.11 to −0.02 e), while the charges of the sulfur and the remaining carbon atoms vary from slightly negative to slightly positive, depending on their surroundings in the crystal.

To investigate the nature of the S···S interactions, we have analyzed the DED map in the plane containing the molecules assembled into an infinite chain by two independent S(1)···S(2) contacts. As one can see from Figure 14A, these interactions can be described as belonging to the so-called "peak−hole" type for which the DED maximum of one sulfur atom is directed toward the area of DED depletion in the vicinity of the other. The same conclusion can be drawn based on the electron localization function (ELF)[27] that is independent of the reference function, e.g., the promolecule used for calculation of the DED. To obtain the ELF function from the experimental XRD data, Tsirelson's approach[28] has been used in which the kinetic energy density is estimated by means of Kirznits's approximation.[29] The applicability of this method to analysis of electron lone pair domains on the basis of XRD data has been proven in a number of investigations.[28,30] The peculiarities of ELF distribution in the plane mentioned above are characterized by the same features as those of DED and are rather close to those observed, e.g., in the crystal of Cl_2.[28,31] Thus we can conclude that interactions of the S···S type can be described in terms of charge transfer from the Lp of one sulfur atom to the antibonding σ-orbital of the S−C bond with participation of the other sulfur atom involved in this interaction. However, from such a qualitative picture it is almost impossible to deduce the direction of charge transfer for each of the S···S contacts. In contrast, for the interactions inside the columns and, in particular, for the S···C ones, such maps clearly show that these interactions

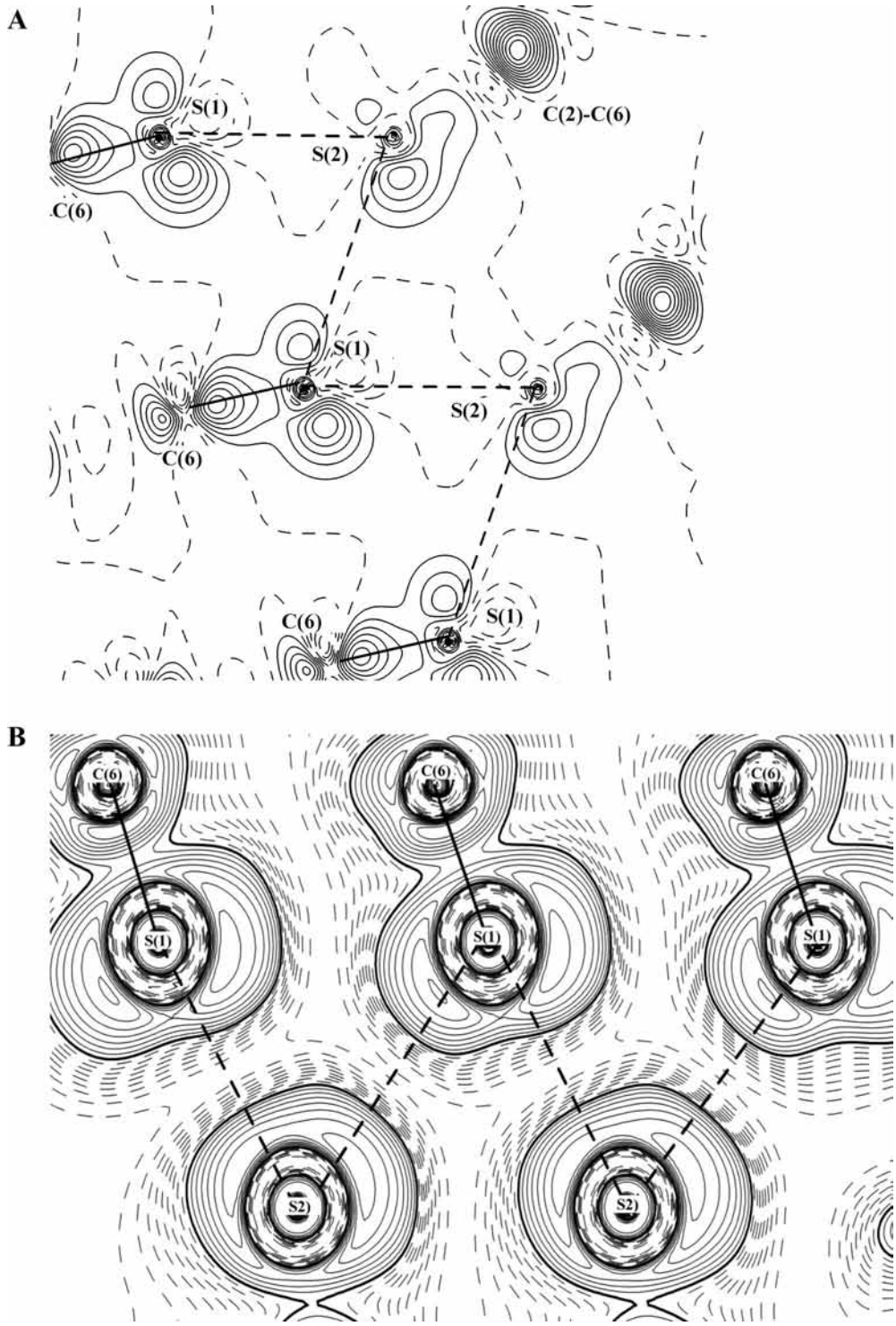

Figure 14. DED map (A) and ELF (B) distribution for S(1)···S(2) interactions. ELF contours are drawn with a 0.05 Å step; the values of ELF less than 0.5 are dashed lines and the value equal to 0.5 is marked by bold lines.

can be described as charge transfer from the sulfur toward carbon atoms (Figure 15). Indeed, as can be seen from the DED map for interactions of two types, namely S(1)···C(2) and C(3)···C(6), both are characterized either by polarization of Lp of S(1) toward DED depletion in the vicinity of the C(2) atom or by polarization of the maximum, corresponding to the C(2)−C(3) bond, toward DED depletion in the vicinity of the C(6) atom. Thus, we can conclude that nonequivalence of sulfur charges, variation of topological parameters in the CPs (3,−1) of the S−C bonds, and nonequivalence of the maxima corresponding to the two lone pairs of the sulfur atom (Figure 13B) are consequences of the charge transfer due to the S···S, S···C, and C···C interactions.

The AIM critical point search for interatomic contacts in the crystal of **1R** has revealed that CPs (3,−1) are located in the area of the S···S contacts with the interatomic separation up to 3.891 Å (Table 1). The number of S···S interactions for each of the independent atoms is different, with only one interaction in the case of the S(3) atom. Inside the columns, the most CPs (3,−1) were found for the S···C contacts; this was confirmed by analysis of the bond paths (Tables 1 and 2).

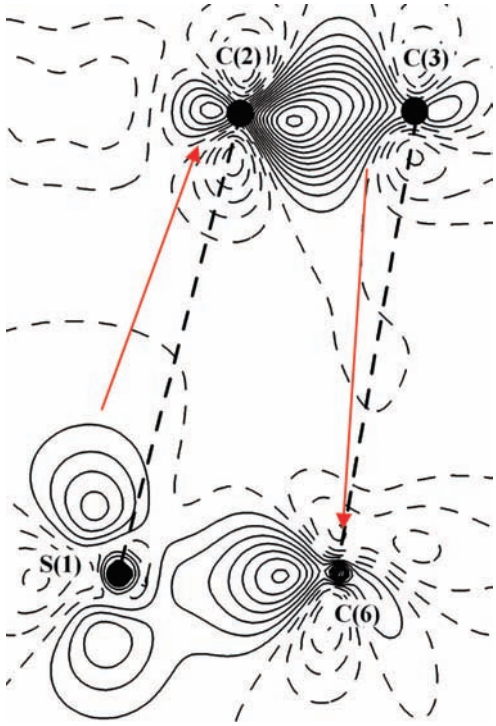

Figure 15. DED map in the plane of the S(1)−C(6) and C(2)−C(3) bonds of two adjacent molecules in the column.

Comparison of topological parameters and, in particular, the values of $\rho(\mathbf{r})$ in CPs (3,−1) clearly shows that the S···S interactions are significantly stronger than the C···C and S···C ones. The shortest C(6)S(1)···S(2)C(6) (1/2 + x, 1/2 + y, −1/2 − z) contact in **1R** is characterized by a $\rho(\mathbf{r})$ value being as much as 0.096 e Å^{-3}; this exceeds analogous values for the S···S contacts in the octasulfur iodoform crystal, where the maximum $\rho(\mathbf{r})$ value for the S···S contact of 3.3536 Å length was 0.086 e Å^{-3},[17] and in 2-thiouracil with its corresponding values of 3.636 Å and 0.03 e Å^{-3}.[19]

Despite their rather high $\rho(\mathbf{r})$ values in CPs (3,−1), the S···S interaction and all the other interactions in **1R** correspond to a closed-shell type; i.e., the electron energy density in CP (3,−1) is positive. To estimate the intermolecular contact energy (E_{cont}), we have used Espinosa's correlation scheme. As seen from Tables 1 and 2, the interaction energies in the crystal **1R** are rather high, varying within the limits 0.54−2.50 kcal/mol. The highest value is observed for the shortest S(1)···S(2) contact, and the minimum one is observed for the extremely long [3.892(1) Å] S(1)···S(4) contact. It is worthy of note that the total energy of interactions for independent S(1), S(2), S(3), and S(4) atoms is significantly different and is equal to 4.5, 6.5, 1.7, and 3.1 kcal/mol, respectively As for the π-stacking interactions, the energy values for the S···C interactions are slightly higher than those for the corresponding C···C ones. The values obtained are close to the results of estimation of the S···S contact energy in the octasulfur iodoform crystal mentioned above.[17] Theoretical estimations of the energy of S···π-system interactions (∼0.8 kcal/mol) in various biological systems[32] also agree well with our results.

The summation of E_{cont} for the S···S, S···C, and C···C bonding interactions listed in Tables 1 and 2 with the account of the C_i site group in the crystal **1R** leads to a lattice energy value equal to 28.5 kcal/mol with overall 88% contribution from the S···S and S···C interactions. This value obtained for the crystal lattice energy of a molecule which does not contain hydrogen atoms can be considered very high. Obviously, this is the reason for the severe conditions of **1R** sublimation and for its insolubility in common solvents.

Although the estimated energies cannot be directly related to the charges of sulfur atoms, it is notable that the highest negative charge is observed for the C(6) and C(8) atoms (−0.11 and −0.10 e). Both these atoms are involved in rather strong S···S contacts in which, according to the SSC angle values, the charge is transferred to antibonding orbitals of the S−C(6) and S−C(8) bonds. The significantly lower absolute value of the C(7) atom charge (−0.03) clearly shows that the charge transfer due to the S···C interactions is distinctly smaller than that for the S···S ones.

The strong S···S interactions present in the crystal **1R** can easily explain the Davydov splittings of vibrational bands, corresponding to normal modes with significant participations of sulfur atoms. Finally, these interactions, involving a high degree of charge transfer, are unambiguously a rational of the red coloration of **1R**. Moreover, the results of charge density analysis also explain the difference between the XRD patterns of **1W** and **1R**. Indeed, a broadening of the (031) reflection in the diffraction pattern of **1W** agrees well with the fact that in **1R** this reflection corresponds to the plane which passes through the atoms S(3)···S(3A) (Figure 4B). Taking into account that the S(3) atom at 100 K forms a minimum number of interactions, interconnecting the columns, it is reasonable to assume that at room or higher temperatures just these interactions can become weaker or even vanish, favoring the libration of molecules about the column axis with respect to the S(3)···S(3A) line. Thus, the main difference between the two modifications is a considerable weakening of S···S interactions.

After rationalizing all the results obtained for **1** by use of different methods, it was reasonable to suppose that **1W**, in contrast to **1R**, could be soluble in common organic solvents. Indeed, **1W** has appeared soluble in hexane. The UV−vis spectrum obtained for this solution is presented in Figure 11.1; it exhibits bands with λ_{max} at 227, 268, and 302 nm, which are slightly shifted in comparison with those of solid **1W** but agree well with the computed data given above, confirming no absorption in the visible region. The fact of **1W** solubility is extremely important, clearing the way to the study of **1** chemistry and formation of thin films suitable for investigation of their electrooptical properties.

Conclusion

Sublimation of octathio[8]circulene $C_{16}S_8$ (**1**) on heating under high vacuum (∼10^{-5} Torr) has led to successive formation of its two modifications: a white film **1W** and a polycrystalline red powder **1R**, depending on heating temperature. When kept for weeks at room temperature, **1W** slowly turns pink, which seems to reflect a monotropic phase transition from a metastable modification to a stable crystalline one.

Single crystal X-ray analysis of **1R** has shown that molecule **1** is planar with nearly equalized C−C as well as C═C and C−S bond distances. Comparison of the results of group-theoretical analysis of vibrational normal modes with the experimental Raman and IR spectra of **1R** has shown that the vibrational spectrum in general obeys the selections rules for the free molecule with the mutual exclusion rule holding true. Crystal field effects in the spectra of **1R** manifest themselves only as Davydov doublets observed for some bands and as a presence of several weak features corresponding to forbidden modes.

Analysis of the electron density distribution in **1R** based on the high-resolution single crystal XRD data and AIM theory

TABLE 1: Geometric, Topological, and Energetic Characteristics of S···S Interactions in the Crystal 1R

X−S···S′−Y	S···S, Å	XSS′, deg	SS′Y, deg	$\rho(\mathbf{r})$, e Å^{-3}	$\nabla^2\rho(\mathbf{r})$, e Å^{-5}	$v(\mathbf{r})$, au	E_{cont},[a] kcal/mol
C(6)S(1)···S(2)C(6) (1/2 + x, 1/2 + y, −1/2 − z)	3.187(1)	168.3(1)	149.1(1)	0.096	0.92	−0.007 96	2.50
C(6)S(1)···S(1)C(6) (−1/2 + x, 1/2 + y, −1/2 − z)	3.540(1)	120.4(1)	135.5(1)	0.065	0.63	−0.004 69	1.47
C(5)S(1)···.S(4)(C5) (3/2 − x, −1/2 + y, 1/2 − z)	3.892(1)	167.2(1)	124.7(1)	0.031	0.29	−0.001 72	0.54
C(7)S(2)···S(4)C(8) (3/2 − x, −1/2 + y, 1/2 − z)	3.501(1)	170.4(1)	120.0(1)	0.062	0.59	−0.004 35	1.36
C(7)S(2)···S(4)C(8) (1/2 − x, −1/2 + y, 1/2 − z)	3.512(1)	121.7(1)	164.0(1)	0.057	0.53	−0.003 84	1.20
C(7)S(3)···S(3)C(7) (1 − x, 1 − y, 1 − z)	3.321(1)	164.2(1)	164.2(1)	0.073	0.7	−0.005 46	1.71

[a] The values of E_{cont} (intermolecular contact energy) were calculated with the use of Espinosa's correlation scheme; $v(\mathbf{r})$ = potential energy density.

TABLE 2: Geometric, Topological, and Energetic Characteristics for S···C and C···C Interactions inside the Columns in the Crystal 1R

X···Y	d, Å	$\rho(\mathbf{r})$, e Å^{-3}	$\nabla^2\rho(\mathbf{r})$, e Å^{-5}	$v(\mathbf{r})$, au	E_{cont}, kcal/mol
S(1)···C(2)	3.647(1)	0.048	0.45	−0.003 06	0.96
S(2)···C(7)	3.519(1)	0.051	0.48	−0.003 32	1.04
S(3)···C(7)	3.653(1)	0.042	0.40	−0.002 6	0.82
S(4)···C(8)	3.510(1)	0.051	0.49	−0.003 35	1.05
C(3)···C(4)	3.508(1)	0.043	0.38	−0.002 55	0.80
C(4)···C(6)	3.582(1)	0.043	0.38	−0.002 58	0.81

SCHEME 1: Modified Synthesis of Sulflower via Bithiophene 5

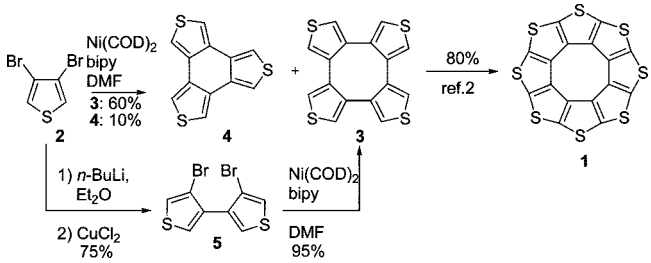

has revealed strong interatomic interactions of π-stacking and charge transfer types with a high overall energy of 28.5 kcal/mol. Due to these strong interactions, **1R** is insoluble, is hard to sublime, and acquires a red color. The latter is reflected by its UV−vis spectrum containing absorption bands in the visible region, in contrast to **1W**. The results of all our studies have shown that **1W** is less ordered than **1R** and exhibits weakened intermolecular interactions. That is why **1W** was supposed to be soluble, and these expectations were justified. Solubility of **1W** has opened the way to the study of chemical and optoelectronic properties of **1** in more detail.

Experimental Section

Synthesis of 1 and Its Precursors. 1 was prepared from cyclic tetrathiophene **3** as described previously.[10] The most convenient method reported to prepare cyclic tetrathiophene **3** (key precursor for the synthesis of sulflower) is oligocyclization of 3,4-dibromothiophene **2** with an equimolar amount of bis(1,5-cyclooctadiene)nickel/2,2′-bipyridine (Ni(COD)$_2$/bipy) system.[10,33] The reaction mixture is hard to separate by column chromatography due to the similar nature of **3** and byproducts. This interferes with the low solubility of **3** in hexane and other nonpolar eluents. It was shown recently that cyclotetramerization of **2** is basically accompanied by formation of the corresponding trimer **4**, with the ratio of **3** to **4** being varied with the ligand nature (2,2′-bipyridine or Ph_3P).[34]

To avoid difficulties with purification, we have improved the method preparation of **3** as follows (see Scheme 1): 3,4-dibromothiophene was converted into 4,4′-dibromo-3,3′-bithiophene **5** by Li−Br exchange followed by oxidative homocoupling with $CuCl_2$.[35] The cyclodimerization of **5** into **3** proceeds with Ni(COD)$_2$/bipy almost quantitatively. The only admixture is the starting **5** if unreacted which can be separated easily by washing with hexane. Interestingly, when **5** was treated with half of the required amount of Ni(COD)$_2$/bipy complex, the only products detected by GC/MS were the starting **5** and the target **3**.

In light of sulflower's outstanding solid state structural properties, one can expect a demand for reliable scaleable and simple method to **3**. The proposed method permits one to avoid column chromatography and to use only half of the otherwise taken amount of the expensive Ni(COD)$_2$.

Single Crystal X-ray Analysis. Crystals of **1R** (red needles, $C_{16}S_8$, M = 448.64) are monoclinic, space group $P2_1/n$, at 100 K: a = 3.8664(1), b = 16.5115(2), c = 11.1393(2) Å, β = 94.0035(8)°, V = 709.40(2) Å^3, Z = 2 (Z' = 0.5), d_{calc} = 2.100 g cm^{-3}, μ(Mo Kα) = 12.52 cm^{-1}, F(000) = 448. Intensities of 83 968 reflections were measured with a Smart APEX II CCD diffractometer [λ(Mo Kα) = 0.710 72Å, ω-scans, $2\theta < 100°$], and 7374 independent reflections were used in further refinement. The structure was solved by direct method and refined by the full-matrix least-squares technique against F^2 in an anisotropic−isotropic approximation. The refinement converged to wR2 = 0.0754 and GOF = 1.046 for all independent reflections (R1 = 0.0328 was calculated against F for 5632 observed reflections with $I > 2\sigma(I)$). All calculations were performed using SHELXTL-Plus 5.0.[36]

The multipole refinement was carried out within the Hansen−Coppens formalism[38] using the XD program package[37] with the core and valence electron density derived from the wave functions fitted to a relativistic Dirac−Fock solution.[39] The refinement was carried out against F and converged to R = 0.026 34, Rw = 0.0229, and GOF = 1.0456 for 5345 merged reflections with $I > 3\sigma(I)$. All bonded pairs of atoms satisfy the Hirshfeld rigid-bond criteria (the maximum difference of the mean square displacement amplitudes was 7×10^{-4} Å^2). The residual electron density was not more than 0.21 e Å^{-3}. Topological analysis of the experimental $\rho(\mathbf{r})$ function was carried out using the WinXPRO program package.[40]

The estimation of the kinetic energy [$g(\mathbf{r})$] was based on the Kirzhnits's approximation[29] relating it to values of the $\rho(\mathbf{r})$ and its derivatives: $g(\mathbf{r}) = (3/10)(3\pi^2)^{2/3}[\rho(\mathbf{r})]^{5/3} + (1/72)|\nabla\rho(\mathbf{r})|^2/\rho(\mathbf{r}) + 1/6\nabla^2\rho(\mathbf{r})]$.

The use of this relationship in conjunction with the virial theorem ($2g(\mathbf{r}) + v(\mathbf{r}) = 1/4\nabla^2\rho(\mathbf{r})$)[15,26] provided the value of potential energy density [$v(\mathbf{r})$] in the critical points from experimental diffraction data. Moreover, this method allowed one to estimate the atomic energy by integration of electron energy density function $h_e(\mathbf{r}) = g(\mathbf{r}) + v(\mathbf{r})$ over the atomic basin (see, e.g., refs 41 and 42).

Powder XRD Measurements. Powder X-ray diffraction (XRD) measurements were carried out using a D8 Advance diffractometer with the following parameters: generator operated

at 40 kV × 40 mA, Cu K$\alpha_{1,2}$ radiation (λ_{av} = 1.5418 Å), Θ/2Θ step scanning mode with a step size of 0.02° and an integration time of 20 s per point, angle range 5 < 2Θ < 60°, T = 295 K, and parallel beam geometry realized with a multilayer Göbel mirror. For the measurements, the polycrystalline powder was deposited onto a single crystalline Si(100) plate. The procedure used for the film preparation is described above. The position of the reflection (200) (32.96° for Cu Kα_1 component) of the silicon substrate, which is theoretically forbidden but nevertheless is characterized by an appreciably high intensity, was used for the angular scale calibration for both types of samples. The experimental patterns were analyzed using the DIFFAC^{plus} program suite.[43]

IR Spectra. IR spectra were registered in the region of 150−3700 cm^{-1} using a Carl Zeiss M-82 spectrophotometer and a Nicolet Magna IR-750 FTIR spectrometer. The samples were KBr pellets as well as thin films sublimed on CsI plates under the conditions described above.

Raman Spectra. Raman spectra in the region 100−3700 cm^{-1} were recorded using a Raman spectrometer of last generation LabRAM with excitation by the red 632.8 nm line of a He−Ne laser with output power less than 5 mW. The spectrometer being equipped with a microscope, we thoroughly picked out suitable microcrystals of **1R** to be able to register Raman spectra of the same microsamples that were used in the X-ray measurements (Figure 2b).

UV−Vis Spectra. UV−vis spectra of solid sulflower and a solution of **1W** in hexane were obtained using a Carl Zeiss M-40 spectrophotometer. Solid samples of **1W** were prepared as thin films sublimed on quartz plates under the conditions described above; the spectra of **1R** were recorded just by smearing and pressing the red polycrystalline substance between two quartz plates.

Computational Methods. Quantum-chemistry calculations of normal-mode frequencies and eigenvectors (in a harmonic approximation) and also of Raman and IR intensities for the free molecule were carried out at the DFT/PBE level with SBK basis set, using the PRIRODA[44] program suite, and also with 6-311G* basis set, using the program suite Gaussian 03;[45] no scaling was applied. Potential energy distribution was computed using the program NCA-99.[46]

Calculation of electronic energy levels of the free molecule was performed at the time-dependent DFT level of theory with a PBE functional and SBK basis set, using the PRIRODA program suite.[44]

NICS indices were computed, in accordance with the recommendation,[24] by the GIAO method at the DFT B3LYP/TZ2P level, using the PRIRODA[44] program suite. The calculation accuracy was checked by reproducing the literature NICS(1) value for benzene, −10.1.[24]

Acknowledgment. The authors are grateful to the Russian Foundation of Basic Research (Grants 06-03-32753, 06-03-32510-à) and the Foundation of the President of the Russian Federation (Federal Program for the Support of Young Doctors, Grants MD-172.2008.3, MK-3894.2007.3).

Note Added in Proof. When our manuscript had been submitted, the paper of T. Fujimoto, R. Suizu, H. Yoshikawa, and K. Awaga (*Chem. Eur. J.* **2008**, *14*, 6053) became available in which the routine single crystal X-ray diffraction data for the title $C_{16}S_8$ compound were reported. The space group determined coincides with our data, and the overall molecular geometry is much the same; however, due to lower resolution and accuracy (R = 0.0842), the C–C bonds of the inner ring were reported there as alternated, which is not confirmed by our high-resolution data.

Supporting Information Available: Tables giving bond lengths and angles, topological parameters in critical points (3,−1), atomic charges, and volumes, parameters of selected diffraction peaks in the powder XRD patterns, and detailed analysis of the vibrational spectrum on the basis of computed and experimental data are presented. This material is available free of charge via the Internet at http://pubs.acs.org. Crystallographic data (excluding structure factors) for the structures reported in this paper have been deposited with the Cambridge Crystallographic Data Center as supplementary no. CCDC-685932. Copies of the data can be obtained free of charge on application to CCDC, 12 Union Road, Cambridge CB2 1EZ U.K. (Fax: (international) +44-1223/336-033; E-mail: deposit @ccdc.cam.ac.uk).

References and Notes

(1) Sun, Y.; Liu, Y.; Zhu, D. *J. Mater. Chem.* **2005**, *15*, 53–65.
(2) Perepichka, I.; Perepichka, D.; Meng, H.; Wudlt, F. *Adv. Mater.* **2005**, *17*, 2281–2305.
(3) Barbarella, G.; Melucci, M.; Sotgiu, G. *Adv. Mater.* **2005**, *17*, 1581–1593.
(4) Nenajdenko, V. G.; Sumerin, V. V.; Chernichenko, K. Yu.; Balenkova, E. S. *Org. Lett.* **2004**, *6*, 3437–3439.
(5) Osuna, R. M.; Ortiz, R. P.; Delgado, M. C. R.; Nenajdenko, V. G.; Sumerin, V. V.; Balenkova, E. S.; Hernandez, V.; Navarette, J. T. L. *ChemPhysChem* **2007**, *8*, 745–750.
(6) Osuna, R. M.; Ortiz, R. P.; Hernandez, V.; Navarette, J. T. L.; Miyasaka, M.; Rajca, S.; Rajca, A.; Glaser, R. *J. Phys. Chem. C* **2007**, *111*, 4854–4860.
(7) Miyasaka, M.; Rajca, A. *J. Org. Chem.* **2006**, *71*, 3264–3266.
(8) Miyasaka, M.; Rajca, A.; Pink, M.; Rajca, S. *J. Am. Chem. Soc.* **2005**, *127*, 13806–13807.
(9) Rajca, A.; Pink, M.; Wang, H.; Rajca, S. *J. Am. Chem. Soc.* **2004**, *126*, 15211–15222.
(10) Chernichenko, K. Yu.; Sumerin, V. V.; Shpanchenko, R. V.; Balenkova, E. S.; Nenajdenko, V. G. *Angew. Chem., Int. Ed.* **2006**, *45*, 7367–7370.
(11) Datta, A.; Pati, S. K. *J. Phys. Chem. C* **2007**, *111*, 4487–4490.
(12) Gahungu, G.; Zhang, J. *Phys. Chem. Chem. Phys.* **2008**, *10*, 1743–1747.
(13) Pykko, P. *Chem. Rev.* **1997**, *97*, 597–636.
(14) (a) Lyssenko, K. A.; Nelyubina, Yu. V.; Kostyanovsky, R. G.; Antipin, M. Yu. *ChemPhysChem* **2006**, *7*, 2453–2455. (b) Lyssenko, K. A.; Korlyukov, A. A.; Golovanov, D. G.; Ketkov, S. Yu.; Antipin, M. Yu. *J. Phys. Chem. A* **2006**, *110*, 6545–6551. (c) Lyssenko, K. A.; Korlyukov, A. A.; Antipin, M. Yu. *Mendeleev Commun.* **2005**, 90–92. (d) Glukhov, I. V.; Lyssenko, K. A.; Korlyukov, A. A.; Antipin, M. Yu. *Faraday Discuss.* **2007**, *135*, 203–215.
(15) Bader, R. F. W. *Atoms In Molecules. A Quantum Theory*; Clarendon Press: Oxford, 1990; 395 pp.
(16) (a) Koritsanszky, T. S.; Coppens, P. *Chem. Rev.* **2001**, *101*, 1583–1628. (b) Gatti, C. *Z. Kristallogr.* **2005**, *220*, 399–457. (c) Tsirelson, V. G.; Ozerov, R. P. *Electron Density and Bonding in Crystals: Principles, Theory and X-Ray Diffraction Experiments in Solid State Physics and Chemistry*; IOP Publishing Ltd.: Bristol, U.K., 1996; 517 pp.
(17) Wolstehholme, D. J.; Robertson, K. N.; Gonzalez, E. M.; Cameron, T. S. *J. Phys. Chem. A* **2006**, *110*, 12636–12643.
(18) Zhikol, O. A.; Shishkin, O. V.; Lyssenko, K. A.; Leszczynski, J. *J. Chem. Phys.* **2005**, *122*, 1–8.
(19) Munshi, P.; Guru Row, T. N. *Acta Crystallogr.* **2006**, *B62*, 612–626.
(20) (a) Espinosa, E.; Molins, E.; Lecomte, C. *Chem. Phys. Lett.* **1998**, *285*, 170–173. (b) Espinosa, E.; Alkorta, I.; Rozas, I.; Elguero, J.; Molins, E. *Chem. Phys. Lett.* **2001**, *336*, 457–461.
(21) Destro, R.; Soave, R.; Barzaghi, M.; Prestjr, L. L. *Chem.—Eur. J.* **2005**, *11*, 4621–4634.
(22) Howard, S. T.; Krygowski, T. M. *Can. J. Chem.* **1997**, *75*, 1174–1181.
(23) von R. Schleyer, P.; Maerker, C.; Dransfeld, A.; Jiao, H.; van, E; Hommes, N. J. R. *J. Am. Chem. Soc.* **1996**, *118*, 6317–6318.
(24) Chen, Zh.; Wannere, C. S.; Corminboeuf, C.; Puchta, R.; von R. Schleyer, P. *Chem. Rev.* **2005**, *105*, 3842–3888.
(25) Fallah-Bagher-Shaidaei, H.; Wannere, C. S.; Corminboeuf, C.; Puchta, R.; von R. Schleyer, P. *Org. Lett.* **2006**, *8*, 863–866.
(26) Bader, R. F. W. *J. Chem. Phys. A* **1998**, *102*, 7314–7323.

(27) Savin, A.; Silvi, B.; Colonna, F. *Can. J. Chem.* **1996**, *74*, 1088–1096.
(28) Tsirelson, V.; Stash, A. *Chem. Phys. Lett.* **2002**, *351*, 142–148.
(29) Kirzhnits, D. A. *Sov. Phys. JETP* **1957**, *5*, 64–70.
(30) (a) Lyssenko, K. A.; Grintselev-Knyazev, G. V.; Antipin, M. Yu. *Mendeleev Commun.* **2002**, 128–130. (b) Lyssenko, K. A.; Antipin, M. Yu.; Gurskii, M. E.; Bubnov, Yu. N.; Karionova, A. L.; Boese, R. *Chem. Phys. Lett.* **2004**, *384*, 40–44.
(31) Tsirelson, V. G.; Zou, P. F.; Tang, T. H.; Bader, R. F. W. *Acta Crystallogr.* **1995**, *A51*, 143–153.
(32) Meyer, E. A.; Castellano, R. K.; Diederich, F. *Angew. Chem., Int. Ed.* **2003**, *42*, 1210–1250.
(33) Zhou, Z.; Yamamoto, T. *J. Organomet. Chem.* **1991**, *414*, 119–127.
(34) Patra, A.; Wijsboom, Y. H.; Shimon, L. J. W.; Bendikov, M. *Angew. Chem., Int. Ed.* **2007**, *46*, 8814–8818.
(35) Gronowits, S. *Acta Chem. Scand.* **1961**, *15*, 1393–1395.
(36) Sheldrick, G. M. *SHELXTL-Plus Reference Manual*, Version 5.0; Siemens Analytical X-ray Instruments Inc.: Madison, WI, 1996.
(37) Volkov, A.; Macchi, P.; Farrugia, L. J.; Gatti, C.; Mallinson, P.; Richter, T.; Koritsanszky, T.; XD2006- *A Computer Program Package for Multipole Refinement and Topological Analysis of Charge Densities and Evaluation of Intermolecular Energies from Experimental and Theoretical Structure Factors*; 2006.
(38) Hansen, N. K.; Coppens, P. *Acta Crystallogr.* **1978**, *A34*, 909–921.
(39) Su, Z.; Hansen, N. K. *Acta Crystallogr.* **1998**, *A54*, 646–652.
(40) (a) Stash, A.; Tsirelson, V. *WinXPRO, a Program for Calculating Crystal and Molecular Properties Using Multipole Parameters of the Electron Density,* rev. 1.5.44; Moscow, 2007. (b) Stash, A.; Tsirelson, V. G. *J. Appl. Crystallogr.* **2002**, *35*, 371–373.
(41) Zhurova, E. A.; Tsirelson, V. G.; Stash, A. I.; Yakovlev, M. V.; Pinkerton, A. A. *J. Phys. Chem. B* **2004**, *108*, 20173–20179.
(42) Tsirelson, V. G. *Acta Crystallogr.* **2002**, *B58*, 632–639.
(43) *DIFFRAC^{plus}*, release 2006; Bruker AXS Inc.: 5465 East Cheryl Parkway, Madison, WI 53711-5373, 2006.
(44) (a) Laikov, D. N. *Chem. Phys. Lett.* **1997**, *281*, 151–156. (b) Laikov, D. N. *Chem. Phys. Lett.* **2005**, *416*, 116–120. (c) Laikov, D. N.; Ustynyuk, Y. A. *Russ. Chem. Bull.* **2005**, *54*, 820–826.
(45) Frisch, M. J.; Trucks, G. W.; Schlegel, H. B.; Scuseria, G. E.; Robb, M. A.; Cheeseman, J. R.; Montgomery, J. A., Jr.; Vreven, T.; Kudin, K. N.; Burant, J. C.; Millam, J. M.; Iyengar, S. S.; Tomasi, J.; Barone, V.; Mennucci, B.; Cossi, M.; Scalmani, G.; Rega, N.; Petersson, G. A.; Nakatsuji, H.; Hada, M.; Ehara, M.; Toyota, K.; Fukuda, R.; Hasegawa, J.; Ishida, M.; Nakajima, T.; Honda, Y.; Kitao, O.; Nakai, H.; Klene, M.; Li, X.; Knox, J. E.; Hratchian, H. P.; Cross, J. B.; Bakken, V.; Adamo, C.; Jaramillo, J.; Gomperts, R.; Stratmann, R. E.; Yazyev, O.; Austin, A. J.; Cammi, R.; Pomelli, C.; Ochterski, J. W.; Ayala, P. Y.; Morokuma, K.; Voth, G. A.; Salvador, P.; Dannenberg, J. J.; Zakrzewski, V. G.; Dapprich, S.; Daniels, A. D.; Strain, M. C.; Farkas, O.; Malick, D. K.; Rabuck, A. D.; Raghavachari, K.; Foresman, J. B.; Ortiz, J. V.; Cui, Q.; Baboul, A. G.; Clifford, S.; Cioslowski, J.; Stefanov, B. B.; Liu, G.; Liashenko, A.; Piskorz, P.; Komaromi, I.; Martin, R. L.; Fox, D. J.; Keith, T.; Al-Laham, M. A.; Peng, C. Y.; Nanayakkara, A.; Challacombe, M.; Gill, P. M. W.; Johnson, B.; Chen, W.; Wong, M. W.; Gonzalez, C.; Pople, J. A. *Gaussian 03*, revision B.03; Gaussian Inc.: Pittsburgh, PA, 2003.
(46) Sipachev, V. A. *J. Mol. Struct. (THEOCHEM)* **1985**, *121*, 143–154.

JP806134U